

Article

Bending Performance of Precast Ceramsite-Concrete-Insulated Sandwich Panel with Stainless Steel Shear Connectors

Yingjie Chen , Chaofeng Kang, Yunfeng Wu and Zhenxiao Qian

College of Hydraulic and Civil Engineering, Xinjiang Agricultural University, Wulumuqi 830052, China

* Correspondence: chenyj2021@xjau.edu.cn

Abstract: With the continuous improvement of building energy-conservation requirements, both traditional concrete external insulation and internal insulation have been unable to meet energy-saving needs. In order to meet the demands of building energy-saving in the new era, new precast concrete external-wall-insulation technology should be developed. In this study, a bending static test and numerical simulation were carried out to evaluate the influence of the thickness of inner concrete wythe and insulation and the length of plate-type shear connectors on the cracking condition, bearing capacity and composite degree of a precast ceramsite-concrete-insulated sandwich panel (PCCISP) under the outside-plane load. The results show that the failure modes of four precast ceramsite-concrete-insulated sandwich panels were all ductile failure of the concrete flexural members. The ultimate bearing capacity of the PCCISP decreased with the decrease in the thickness of the inner concrete wythe. Reducing the thickness of insulation had no significant influence on the ultimate bearing capacity. When the thickness of insulation was reduced by 30%, the composite degree of rigidity and bearing capacity of the PCCISP were increased by 8.85% and 2.67%, respectively. Increasing the length of the plate-type shear connector slightly increased the ultimate bearing capacity, but it had no obvious influence on the rigidity and bearing capacity composite degree.

Keywords: precast ceramsite-concrete-insulated sandwich panel (PCCISP); stainless steel shear connector; bending performance test; composite degree; finite-element analysis



Citation: Chen, Y.; Kang, C.; Wu, Y.; Qian, Z. Bending Performance of Precast Ceramsite-Concrete-Insulated Sandwich Panel with Stainless Steel Shear Connectors. *Buildings* **2022**, *12*, 1640. <https://doi.org/10.3390/buildings12101640>

Academic Editor: Tomasz Sadowski

Received: 2 August 2022

Accepted: 24 September 2022

Published: 9 October 2022

Publisher's Note: MDPI stays neutral with regard to jurisdictional claims in published maps and institutional affiliations.



Copyright: © 2022 by the authors. Licensee MDPI, Basel, Switzerland. This article is an open access article distributed under the terms and conditions of the Creative Commons Attribution (CC BY) license (<https://creativecommons.org/licenses/by/4.0/>).

1. Introduction

Recently, the construction industry's energy-consumption problem has become more serious, and various countries are advocating energy conservation in construction [1,2]. Of a building's total energy consumption, the energy consumption of the external wall accounts for the vast majority [3]. Strengthening the thermal insulation performance of a building's envelope structure will reduce the loss of energy inside the building, thereby effectively reducing the consumption caused by heating. Therefore, improving the self-insulation performance of the exterior panel is a key development toward achieving building-energy conservation. At present, there are many deficiencies in the performance of existing wall insulation, so finding an external wall panel with good performance and insulative effects is a problem that we need to solve. A new type of precast ceramsite concrete sandwich panel is proposed in this paper. It is a self-insulating panel consisting of two ceramsite concrete panels, a rigid polyurethane insulation layer and some stainless steel shear connectors. Considering that ceramsite has the advantages of heat preservation, earthquake resistance, fire resistance (four times that of ordinary concrete), light weight and so on [4–6], we replace the stones in ordinary concrete with ceramsite as coarse aggregate to make ceramsite concrete, which further improves the thermal insulation performance of wall panels, and thus, can achieve wall self-insulation in a real sense [7,8]. The sandwich insulation layer selects rigid foam polyurethane insulation material with low thermal conductivity, which has excellent thermal insulation performance, fire retardance and other advantages [9,10]. Compared with XPS and EPS, it also has stronger adhesion [11]. The

PCCISP combines the advantages of ceramsite concrete and polyurethane insulation, which not only has a good insulation effect but also strong fire resistance.

In order of ability of shear-force transfer between inner and outer concrete wythes, Einea et al. divided the precast concrete sandwich panel (PCSP) into complete a composite panel, partial composite panel and non-composite panel [12–14], as shown in Figure 1. The complete composite panel refers to the fact that the shear connector has a strong ability to transfer shear force, so that the two concrete wythes form a whole to jointly resist external load. A non-composite panel means that the shear force cannot be transferred by the shear connector, and the inner and outer concrete wythes resist external load. The shear connectors of the partial composite panel can transfer partial shear force, and its composite performance is greater than that of a non-composite panel, but smaller than that of a complete composite panel [15–17].

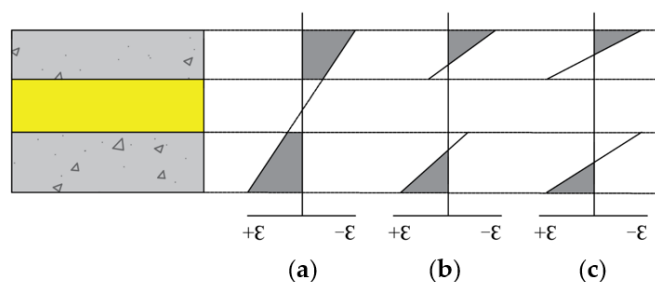


Figure 1. Sectional strain distribution of the sandwich panel: (a) Complete composite; (b) Partial composite; (c) Non-composite.

Therefore, in a sandwich panel, the shear connectors are the key component that determines the interaction between the two concrete wythes. There are many types of shear connector, and stainless steel shear connectors are widely used because of their excellent fire resistance and durability [18]. Stainless steel shear connectors (Figure 2) are generally divided into load-bearing shear connectors and limit shear connectors. Load-bearing shear connectors, such as the plate-type shear connector (Figure 2 right), mainly bear the earthquake load and wind load in-plane. Limit shear connectors, such as the pin-type shear connector (Figure 2 left), mainly play the role of bearing the load outside the plane. The stainless steel shear-connector system is generally composed of vertical load-bearing shear connectors, horizontal load-bearing shear connectors and a number of limit shear connectors.



Figure 2. Detail drawing of stainless steel shear connector.

Many scholars have performed corresponding research on the flexural performance of the PCSPs, sandwich beams and other flexural components. Zhang et al. conducted experimental studies on the failure behavior of geometrically asymmetrical metal foam-core sandwich beams, and the results showed that the initial failure modes of the sandwich beams were strongly related to their geometric characteristics and material properties [19,20]. Additionally, they studied the large deflection of multilayer sandwich beams using analytical and numerical methods, and the analytical solution of the large deflection of multilayer sandwich beams under transverse load was derived. The finite-element result showed that the thickness of the panel and the strength of the foam have great influence on the

plastic behavior of a sandwich beam with multiple layers [21,22]. Bush et al. observed that a PCSP with steel-truss shear connectors had a high degree of combination through the bending test [23]. Huang et al. completed the flexural resistance test of the PCSP with GFRP shear connectors, and it was concluded that the bearing capacity of the sandwich panel could be improved upon by expanding the cross-sectional area of GFRP shear connectors and reducing the layout spacing [24]. Zhi et al. proposed a kind of shear connector and conducted flexural tests on PCSP using this shear connector. They found that the flexural performance of the PCSP was related to the rigidity and strength of the shear connector [25]. O'Hegarty et al. conducted a three-point bending test and finite-element simulation on PCSP with FRP shear connectors, and found that when the thickness of the outer concrete wythe was increased by 15 mm, the ultimate bearing capacity and flexural stiffness of PCSP were doubled [26]. Choi et al. used GFRP shear connectors in the PCSP, and found that the number of shear connectors had an impact on the ultimate bearing capacity of the PCSP [27]. Frankl et al. found that the degree of combination of PCSPs could be improved by increasing the number of CFRP shear connectors [28]. Pessiki et al. studied the influence of adhesive force between the insulation layer and the concrete panel on combination behavior, and the results showed that EPS without shear connectors could provide a 5% compounding effect [29]. Most of the above-mentioned scholars have studied the flexural performance and composition of the PCSP using GFRP and other shear connectors. Although fiber-composite plastic connectors have low thermal conductivity, they have low interlaminar shear strength and are prone to brittle failure, which is also a worrying problem in the case of a fire. The stainless steel shear connectors can solve the above problems, but there are few literature reports on PCSPs with stainless steel shear connectors.

In this paper, a kind of precast ceramsite-concrete-insulated sandwich panel with stainless steel shear connectors is presented. Firstly, four PCCISPs were designed and manufactured to carry out out-of-plane static-loading tests. The bearing capacity, stiffness and failure mode of PCCISPs with different inner-wythe thicknesses, insulation layer thicknesses and plate-type shear connector lengths were observed so as to better understand the structural behavior of the PCCISPs. Thereafter, Abaqus was used for finite-element analysis on the basis of the accuracy of the finite-element model, and the influence of other parameters on the bearing capacity of the PCCISP was further studied. Lastly, the influence of different parameters on the composite degree of the PCCISP was studied via theoretical calculation. This paper provides a reference for the design of a PCCISP with stainless steel shear connectors.

2. Experimental Design

2.1. Description of the Test Specimens

Four PCCISPs were designed in this research, and the static-loading tests were carried out on them. The length and width of the four test panels were the same, with a length of 3000 mm, a span of 2800 mm, a width of 1500 mm and a thickness of 280 mm and 310 mm. The outer concrete wythe was decorated with single-layer bi-directional steel bars, and the inner concrete wythe was decorated with double-layer bi-directional steel bars. The longitudinal and transverse steel bars were both HRB400, with a diameter of 10 mm and a spacing of 200 mm (see Figure 3). The basic parameters of test panels (SP-1~SP-4) are shown in Table 1. Stainless steel shear connectors were used to connect the two concrete wythes of the PCCISPs with the rigid foam polyurethane insulation board of the sandwich layer. The stainless steel shear connectors were arranged in a combination of plate-type shear connectors and pin-type shear connectors. The plate-type shear connectors were symmetrical and the pin-type shear connectors were evenly arranged in the panel (see Figure 4).

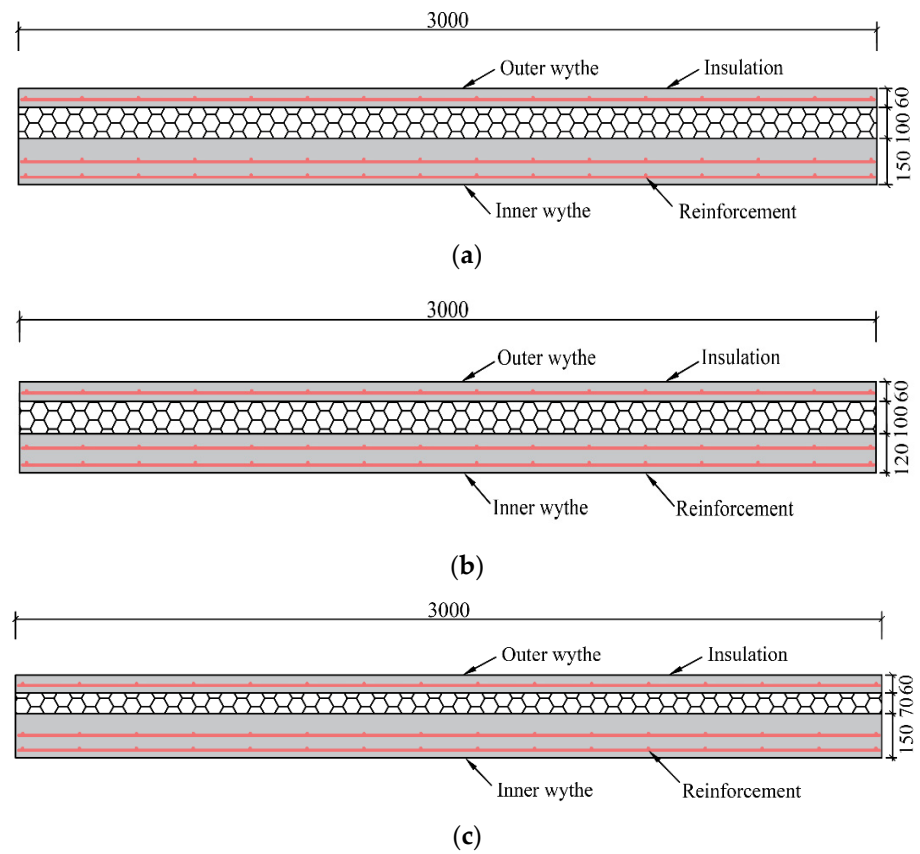


Figure 3. Specimen size and reinforcement: (a) SP-1 and SP-4; (b) SP-2; (c) SP-3.

Table 1. Basic parameters of the specimen.

Panels	Thickness/mm			Length/mm
	Outer Concrete Wythe	Insulation Layer	Inner Concrete Wythe	Plate-Type Shear Connector
SP-1	60	100	150	120
SP-2	60	100	120	120
SP-3	60	70	150	120
SP-4	60	100	150	200

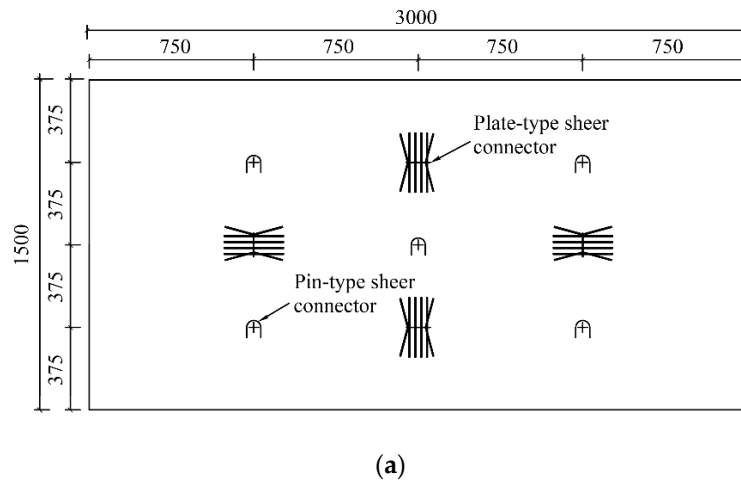


Figure 4. Cont.

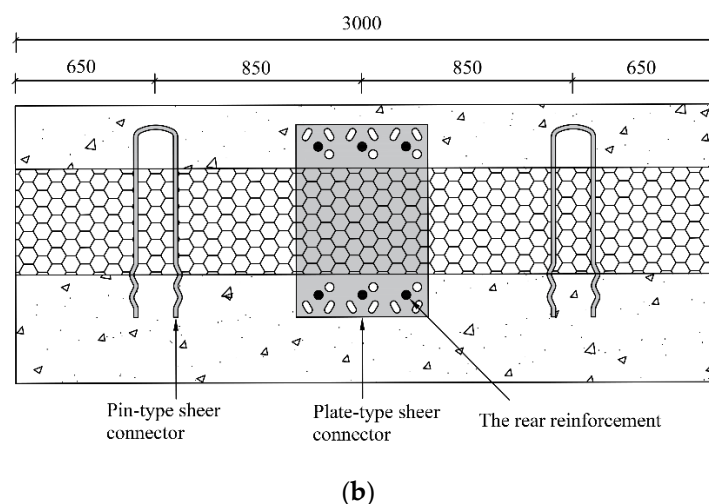


Figure 4. (a) General arrangement of stainless steel connectors; (b) Detailed drawing of stainless steel shear connector.

2.2. Material Mechanical Properties

The compressive strength of the ceramsite-concrete cube tested was 32.6 MPa, the tensile strength was 2.7 MPa, the apparent density was 1827 kg/m^3 and the elastic modulus was $1.99 \times 10^4 \text{ Mpa}$. The yield strength and ultimate tensile strength of a HRP400 steel bar with diameter of 10 mm were 563 MPa and 658 MPa, respectively. The density of the polyurethane insulation layer was 45 kg/m^3 , and the compressive and tensile strengths were 0.35 MPa and 0.42 MPa, respectively. The performance parameters of the two stainless steel shear connectors are shown in Table 2.

Table 2. Performance parameters of stainless steel shear connector.

Type of Shear Connector	Standard Value of Tensile Strength/MPa	The Yield Strength/MPa
Plate-type shear connector	661	405
Pin-type shear connector	858	713

2.3. Loading Scheme and Measuring Point Arrangement

The loading device is shown in Figure 5. The specimens were placed flat and loaded forward. The load was loaded at 5 kN for each level, and the load was held for 10 min after each level was loaded; the loading was stopped when the panels reached the ultimate load standard, and the development of cracks was recorded and observed. Three LVDTs were arranged at both ends and at the midspan of the specimen to measure the midspan deflection. The strain gauge was set up in the middle position and loading position of the tensile-steel-mesh specimen to measure the strain of the steel bars. Two concrete strain gauges were set in the transverse middle position of two concrete wythes to obtain the concrete strain along the height of the section.

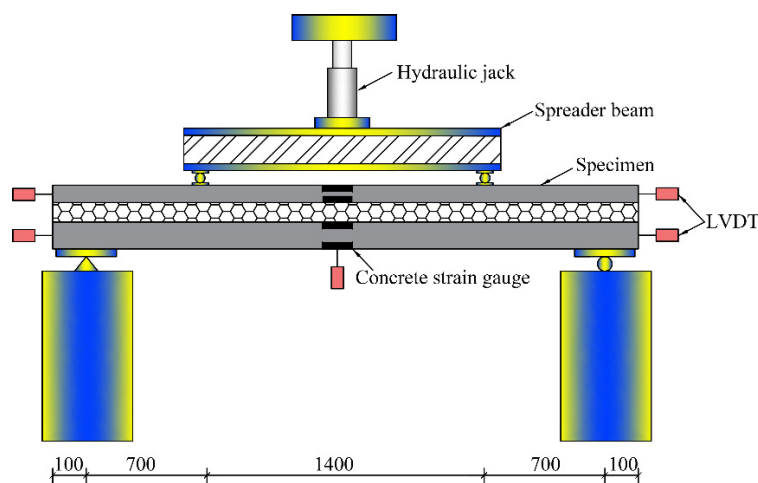


Figure 5. Schematic diagram of test loading device.

3. Test Results and Analysis

3.1. Failure Phenomenon of Specimen

The deformation and crack morphology of SP-1~SP-4 are shown in Figure 6. The failure modes of the four PCCISPs were similar. Taking SP-1 as an example, at the beginning of loading, the overall stiffness of the panel was good due to the small load on the panel surface, and there was no cracking phenomenon. Accompanied by a subtle concrete cracking sound at the bottom of the panel, the first crack appeared in the bottom span of the inner concrete wythe. At this time, the load was 36.32 kN. The overall stiffness of the specimen was good, and the insulation layer of the inner concrete wythe at the right end of the specimen showed a relative slip of about 4 mm. When the load reached 40.19 kN, the outer concrete wythe also cracked. After continued loading, cracks gradually widened and developed along the plate's height. At this time, the maximum width of cracks in the inner and outer concretes wythe were 0.35 mm and 0.25 mm, respectively. When the load reached 82.46 kN, the longitudinal bars in the inner concrete wythe yielded under stress. The conditional ultimate load of 123.80 kN was achieved at a midspan deformation of 56 mm (one fiftieth of the span). When the deflection of the specimen increased to 69 mm, the concrete on the surface of the outer concrete wythe was crushed, showing the failure characteristics of proper reinforcement failure. When SP-1 was destroyed, there was an obvious fracture phenomenon between the inner concrete wythe and the insulation layer, and a slip of 13 mm was generated between the plane-end insulation layer and the inner concrete wythe. The failure phenomena of the specimens are shown in Figure 7.

The inner and outer concrete wythe of SP-2 cracked earlier than that of SP-1, and there were more cracks in the outer concrete wythe. After the test, the right end of the specimen had a slip of 8 mm. The failure phenomenon of SP-1, SP-2 and SP-4 was that the concrete on the surface of the outer concrete wythe was crushed, while that of SP-3 was that the concrete on the surface near the plate-edge was crushed, and the middle part of the loading area showed strip cracking. The slip at the end of specimen WB-3 was smaller than that of WB-1, and the slip amount was 10 mm. The slip produced by SP-4 is not very different from that of specimen SP-1.

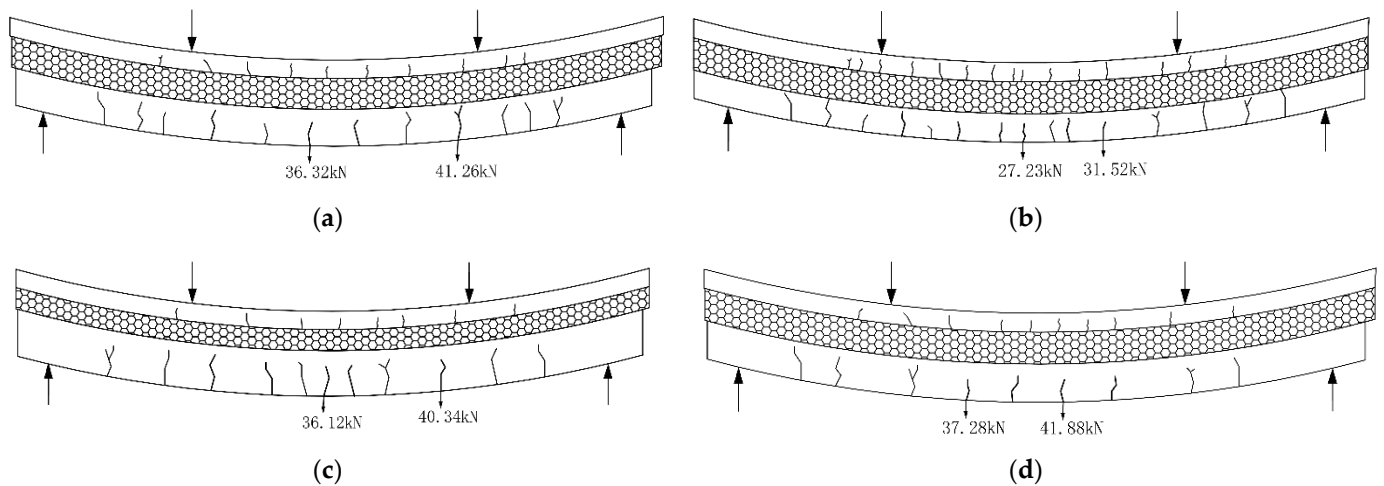


Figure 6. Specimen deformation and crack distribution (The arrow indicates the direction of force): (a) SP-1; (b) SP-2; (c) SP-3; (d) SP-4.



Figure 7. Failure phenomena of SP-1 specimen (Failure phenomenon is in the red circle): (a) Local cracking phenomenon; (b) Local debonding phenomenon.

3.2. Bearing Capacity Analysis

Table 3 shows the bearing-capacity characteristic values of each specimen. As can be seen from Table 3, when comparing SP-1 and SP-2, the thickness of the inner concrete wythe decreased by 20% and the cracking load of the PCCISP decreased by 25.03%. It had a slight impact on yield load, which only reduced by 11.15%, and reduced the ultimate bearing capacity by 9.41%. This was because when the thickness of the inner concrete wythe decreased, the effective section of the PCCISP in terms of thickness decreased, the overall stiffness of the PCCISP decreased and the ultimate bearing capacity of the PCCISP decreased accordingly. Comparing SP-1 and SP-3, the thickness of the insulation layer decreased by 30%, which had little influence on the cracking load and yield load of the PCCISP, and the ultimate bearing capacity only increased by 0.72 kN, reaching 114.54 kN. This was because, in the test process, the debonding phenomenon of the SP-1 insulation layer and the concrete slab occurred earlier, and the insulation layer broke; SP-3, with a smaller insulation-layer thickness, did not show an obvious debonding or fracture phenomena, making the bearing capacity of SP-3 and SP-1 a little different. By comparing SP-1 and SP-4, it can be concluded that the ultimate load was slightly increased when the length of the plate-type shear connectors were increased by 1.67 times.

Table 3. Test results of each specimen.

Panels	Cracking Load/kN	Yield Load/kN	Ultimate Load/kN
SP-1	36.32	82.46	113.82
SP-2	27.23	73.18	103.11
SP-3	36.12	81.78	114.54
SP-4	37.28	83.67	115.58

3.3. Load-Deflection Curve

Figure 8 shows the midspan load-deflection curves of the four PCCISPs. Through the contrast of SP-1 and SP-2 we can see that, before the yielding load, the shape of the two load-deflection curves were similar and showed a linear change. The slope of the curve of SP-2 was obviously lower than that of SP-1, indicating that the flexural stiffness and ductility of SP-2 were much lower than those of SP-1. When the two specimens reached the yield load, the wallboard rigidity began to decline, and the increase in the deflection was obviously greater than the increase in the load. The results show that reducing the thickness of the inner concrete wythe can reduce the flexural stiffness and ductility of the PCCISP. Comparing SP-1 and SP-3, their load-deflection curve trends were basically the same before the cracking load. Before yield load, the rigidity of SP-3 was less than that of SP-1. The slopes of the two curves were basically the same when the yield load was reached. Specimen SP-3 had a long, gently increasing displacement section before peak load, indicating that reducing the thickness of the insulation layer can make the sandwich panel have a good deformation capacity, but this had no obvious influence on the flexural capacity. In contrast with SP-1, the slope of SP-4 was slightly higher before cracking load, indicating that increasing the length of the plate-type shear connector had a small increase in rigidity. After yielding load, the slope of the curve of SP-4 was similar to that of SP-1, indicating that increasing the length of the plate-type shear connector can slightly improve the bending stiffness of the specimen before yielding.

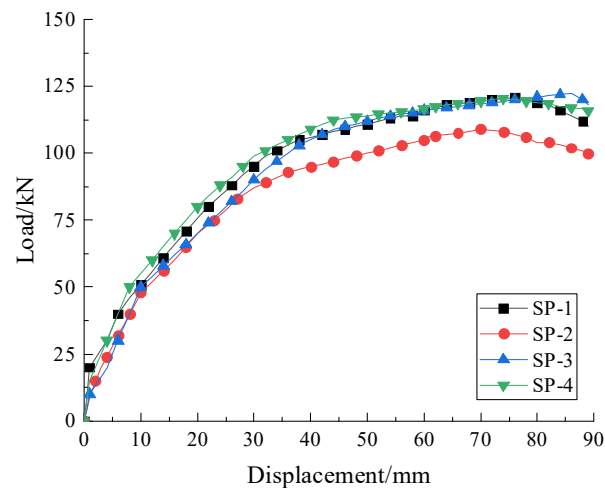


Figure 8. Load-deflection curves of SP-1–SP-4.

3.4. Concrete Strain Analysis

The concrete strain distribution of the midspan sections of the four PCCISPs are shown in Figure 9. It can be found from Figure 9a–d that the four PCCISPs were all partially composite panels. The strain of two concrete wythes before cracking was small, and the strain of SP-3 before cracking was approximately linear along the height of the panel section, which conformed to the assumption of the plane section, and had a high degree of combination. This was due to the load being small before cracking, as the shear force was resisted together by the shear connectors and the bonding force between the insulation layer and the ceramsite-concrete panel. After cracking, the bonding effect gradually disappeared as the load increased. Then, the inner and outer concrete wythes had their own neutralization axes, and the degree of combination also weakened.

As can be seen from SP-1 and SP-2, the neutralization-axis ratio of the outer concrete wythe of SP-2 was lower than that of SP-1, and the neutralization-axis ratio of the inner concrete wythe was higher than that of SP-1. This phenomenon indicates that the composite performance of the PCCISP can be improved by reducing the thickness of the inner concrete wythe. Compared with specimen SP-1, the neutralization axis of the concrete in the outer concrete wythe of SP-3 moved downward with a small amplitude, while the neutralization

axis of the concrete of the inner concrete wythe moved upward slightly. The results show that thinner insulation layers can improve the composite performance of PCCISPs, but the effect is not as good as that obtained by reducing the thickness of inner concrete wythe. According to the comparison of SP-1 and SP-4, the concrete's neutralizing axis of two concrete wythes had almost no obvious movement, which indicated that increasing the length of the plate-type shear connector had no obvious effect on improving the composite performance of the PCCISP.

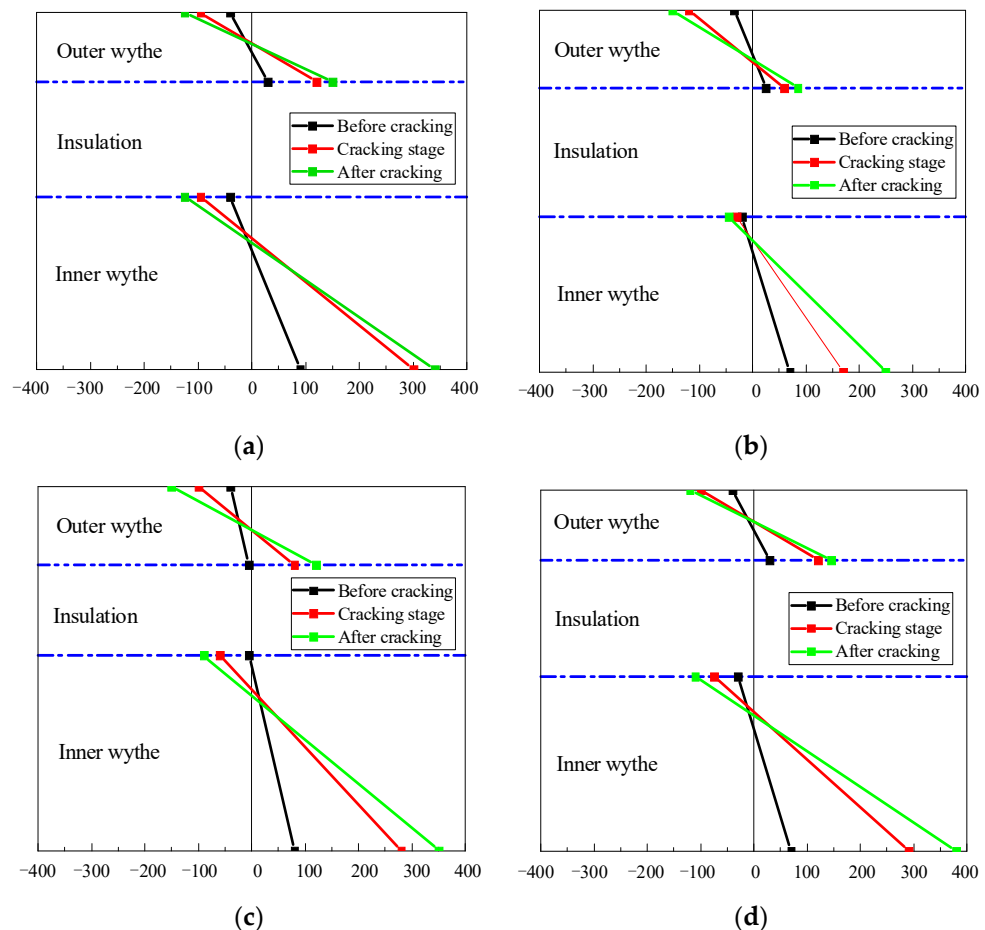


Figure 9. Strain distribution of concrete at midspan section: (a) SP-1; (b) SP-2; (c) SP-3; (d) SP-4.

4. Finite-Element Analysis

4.1. Model Description

Abaqus was used to establish the corresponding three-dimensional finite-element model of the four specimens. Firstly, the concrete and polyurethane materials in the finite-element model were assumed to be homogeneous elastic materials, and the bond-slip between the reinforcement and the concrete was ignored [30]. The “C3D8R” model was used to simulate ceramsite concrete, the polyurethane insulation layer and the plate-type shear connector, the “T3D2” model was used to simulate reinforcement [31] and the “B13” model was used to simulate pin-type shear connectors.

The ceramsite concrete adopted the concrete-damage plastic model. The elastic modulus was 1.99×10^4 MPa, the Poisson's ratio was 0.2 and other parameters are shown in Table 4. The stress–strain relationship was selected according to Chinese code JGJ12-2006, and the formula is as follows:

$$\sigma_c = f_c \left[1.5 \left(\frac{\varepsilon_c}{\varepsilon_0} \right) - 0.5 \left(\frac{\varepsilon_c}{\varepsilon_0} \right)^2 \right] \quad \varepsilon \leq \varepsilon_0 \quad (1)$$

$$\sigma_c = f_c \quad \varepsilon_0 < \varepsilon \leq \varepsilon_{cu} \quad (2)$$

where σ_c is the ceramsite-concrete stress and ε_0 is the strain corresponding to the compressive strength, which is taken as 0.002 in this model.

Table 4. Damage plastic parameters of ceramsite concrete.

Dilation Angle	Eccentricity	f_{b0}/f_{c0}	K	Viscosity Parameter
30	0.1	1.16	0.667	0.0001

The reinforcement adopted the ideal elastic-plastic model. Before reaching the yield strength, the uniaxial tensile stress of the reinforcement has a linear elastic relationship with the strain. After reaching the yield strength, the material enters a plastic stage where the stress remains constant as the strain increases. The elastic modulus was taken as 2.02×10^5 MPa, and the Poisson's ratio was taken as 0.2. The stress–strain relationship of the steel bar is expressed as:

$$\sigma = E_s \varepsilon \quad \varepsilon \leq \varepsilon_y \quad (3)$$

$$\sigma = f_y \quad \varepsilon > \varepsilon_y \quad (4)$$

where E_s and ε_y are the elastic modulus and the yield strain of the reinforcement, respectively.

The elastic modulus of the polyurethane insulation was taken as 36.4 MPa, and the Poisson's ratio was taken as 0.4. The constitutive relation of the stainless steel shear connector adopted the linear isotropic strengthening model. The elastic modulus and Poisson's ratio of stainless steel shear connectors were 2.01×10^5 MPa and 0.3, respectively, and the values are shown in Table 3.

Reinforcing mesh and stainless steel shear connectors were embedded into the concrete. The shear force was mainly imposed by the rear reinforcement through the hole-wall to the shear connectors. Therefore, the normal contact between the rear reinforcement and the circular hole of the plate-type shear connector was defined as “hard” contact, and the friction coefficient of the tangential behavior was set as 0.6. The layout model of the plate-type shear connector is shown in Figure 10. The mesh size of the stainless steel shear connector was 20 mm and the others were 50 mm. The loading mode was consistent with the test, and the boundary conditions of the supports at both ends of the panel were set as simply supported fixed-form [32].

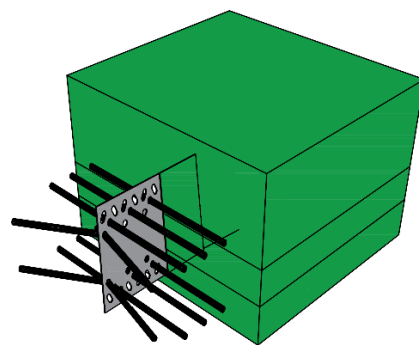


Figure 10. Model drawing of plate-type shear connector.

The simulation of the contact of the insulation layer and the concrete is one of the key points in establishing this model. Contact behaviors in Abaqus mainly include “Tie” and “surface-to-surface” contacts. A “Tie” is used to bind the nodes of two surfaces together, so that the nodes from the surface are constrained to having the same degree of freedom and motion as the corresponding nodes on the main surface [33]. The “surface-to-surface” contact is a special discontinuous constraint, which is used to simulate force-transfer and friction-sliding between contact surfaces [34]. Therefore, this interaction consists of two

parts. First is the normal interaction between contact surfaces; “hard” contact is commonly used to simulate normal behavior, and only when there is no gap between contact surfaces can pressure be transferred; otherwise, the contact effect will not take effect. The second is the tangential behavior between the contact surfaces. In this paper, the frictionless formula and the penalty friction formula based on the “Coulomb friction” model were selected. The penalty friction formula determines the critical shear stress according to the normal contact pressure and friction coefficient μ . When the interface shear stress exceeds this critical value, relative sliding of the contact surface will occur. Three different finite-element models were established for the above three interactions. The first had the surfaces of the insulation layer and concrete adopt the “Tie” connection. The second was to use the “surface-to-surface” contact, with the contact attribute set as a normal “hard” contact and with a tangential friction coefficient of 0.4 penalty function. The third was set up as a “surface-to-surface” contact; the properties were set to “hard” contact in the normal direction and with no friction in the tangential direction. Through the comparison of the three different models above and experimental data, a more-reasonable numerical simulation method could be obtained.

4.2. Finite-Element Model Validation

Figure 11 shows that the “no friction” model is closest to the test values. In fact, in the process of testing, the phenomenon of debonding appeared very early in the concrete panel and the thermal insulation layer, which also proved that the natural bonding force of the concrete board and the thermal insulation layer had little influence on the flexural performance of the components; as such, we did not consider the friction of the interface to be more consistent with the actual situation. Therefore, “no friction” was used to set the interface behaviors of the insulation layer and concrete, and the finite-element model was established.

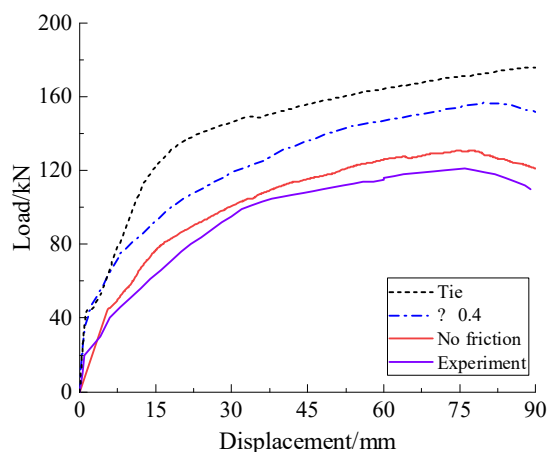


Figure 11. Load-deflection curves of three models and test.

Figure 12 shows the displacement contours of the numerical model of the four PC-CISPs, and Figure 13 shows the load-deflection curves obtained from the finite-element calculations and tests. The comparison between the simulated value of ultimate load and the test value is shown in Table 5. From Figure 13a–d, it can be seen that the simulated curves of the four specimens were basically consistent with the test curves, and the simulated values were slightly larger than the test values. This was because the finite-element model was calculated under ideal conditions, while the actual test would be interfered with by multiple external factors.

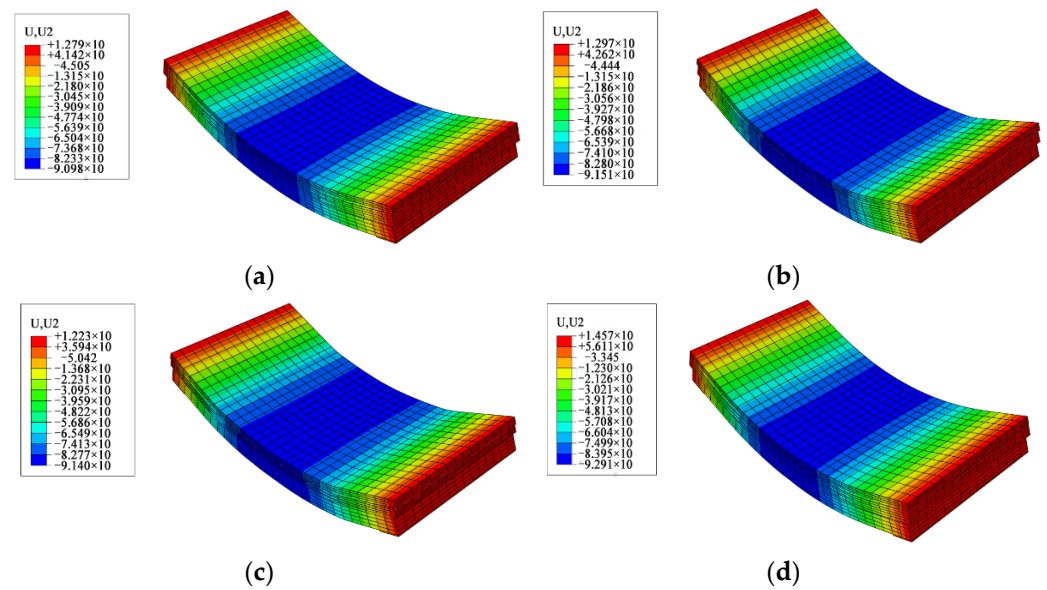


Figure 12. Displacement cloud diagram of finite-element model: (a) SP-1; (b) SP-2; (c) SP-3; (d) SP-4.

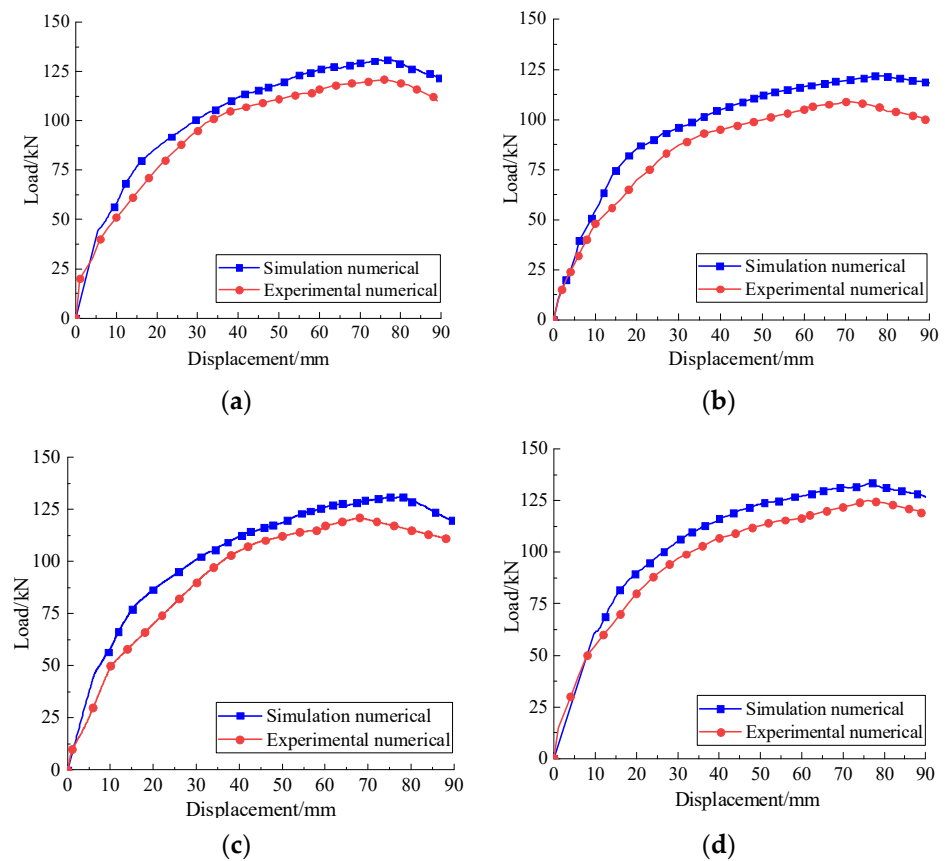


Figure 13. Finite-element analysis and test load-deflection curves: (a) SP-1; (b) SP-2; (c) SP-3; (d) SP-4.

The relative difference between the finite-element simulation and the test in Table 5 was within 9.60% on average. The biggest difference was SP-2, whose experimental ultimate load was 89.77% of the simulated ultimate load, and the smallest difference was SP-4, whose experimental ultimate load was 92.11% of the simulated ultimate load. The results show that the model can accurately reflect the stress of the precast ceramsite concrete sandwich panel, and can be used as a reference for the design of the same type of sandwich panels.

Table 5. Test and simulation values of ultimate load.

Panels	Test Value/kN	Simulation Value/kN	The Relative Difference
SP-1	113.82	123.79	8.76%
SP-2	103.11	114.86	11.40%
SP-3	114.54	124.21	9.67%
SP-4	115.67	125.58	8.57%

4.3. Parameter Analysis

Based on the size of the loaded specimen, the original three parameters and a new parameter were further studied. The original three parameters were the thickness of the inner concrete wythes (100 mm~160 mm), the thickness of the insulation layer (50 mm~160 mm) and the length of plate-type shear connectors (80 mm~240 mm). A new parameter was the number of pin-type shear connectors (10, 15, and 20). A total of 12 specimens were designed. Table 6 shows the parameters and finite-element calculation results of specimens.

Table 6. Finite-element calculation results.

Panels	Thickness/mm			Length/mm	Number	Ultimate Load/kN
	Outer Concrete Wythe	Insulation Layer	Inner Concrete Wythe	Plate-Type Shear Connector	Pin-Type Shear Connector	
SP-2-1	60	100	160	120	5	126.92
SP-2-2	60	100	140	120	5	120.13
SP-2-3	60	100	100	120	5	108.74
SP-3-1	60	160	150	120	5	121.28
SP-3-2	60	130	150	120	5	122.35
SP-3-3	60	50	150	120	5	125.87
SP-4-1	60	100	150	80	5	123.03
SP-4-2	60	100	150	160	5	124.72
SP-4-3	60	100	150	240	5	126.11
SP-5-1	60	100	150	120	10	125.68
SP-5-2	60	100	150	120	15	127.04
SP-5-3	60	100	150	120	20	128.65

It can be seen in Table 6 that the thinner the inner concrete wythe thickness, the smaller the bearing capacity. When the inner concrete wythe thickness decreased by 20 mm, the ultimate bearing capacity decreased to 94.65% on average. The thickness of the insulation layer had a small influence on the flexural capacity of the PCCISP. In addition, when the number of pin-type shear connectors was increased, the flexural bearing capacity of the PCCISP was improved slightly. This is because increasing the number of pin-type shear connectors can increase the connection between the two concrete panels and reduce the movement of the insulation board, so the two concrete panels can bear more force together. From the point of view of engineering applications, when the PCCISP is designed, the thickness of the insulation layer can be reduced appropriately and can be selected rationally under the premise of meeting the design specifications, so as to reduce the engineering cost.

5. Analysis of Composite Degree

The concept of “composite degree” can be defined as the sliding that occurs in the sandwich panel. A complete composite panel with a combination degree of 100% indicates that there is no sliding between the concrete slab and the insulation layer in the sandwich panel [35]. The composite degree of the sandwich panel is different in different stress stages. There are two main methods to calculate it: (1) k_1 is used to represent the composite degree of the specimen before cracking. (2) k_2 is used to represent the composite degree of the specimen after cracking.

The effective moment of inertia of the cracked concrete section (I_e) and the experimental (I_{exp}) of each specimen are calculated using Formulas (5) and (6), respectively:

$$I_e = \left(\frac{M_{cr}}{M_a}\right)I_g + \left[1 - \left(\frac{M_{cr}}{M_a}\right)^3\right]I_{cr} \quad (5)$$

$$I_{exp} = \frac{23Pl^3}{648E\Delta} \quad (6)$$

where M_{cr} is the bending moment when cracking, M_a is the maximum bending moment calculated theoretically, and I_g and I_{cr} are the moment of inertia of the total section and that of the cracked section, respectively.

Before cracking, the sandwich panel is represented by the rigidity composite degree [36]:

$$k_1 = \frac{I_{exp} - I_{nc}}{I_c - I_{nc}} \quad (7)$$

where I_{exp} represents the actual moment of inertia when the ceramsite concrete cracks, and I_{nc} and I_c are the moment of inertia of non-composite panels and complete composite panels, respectively.

It is difficult to calculate the ultimate bearing capacity of the sandwich panel by the conventional theoretical methods, but it can be calculated using the theoretical method when the sandwich panel is complete composite and non-composite [37]. When the sandwich panel is a non-composite panel (Figure 14a), the ultimate flexural capacity is equal to the sum of the flexural capacity of the two concrete panels, since each concrete panel bears its own load. The ultimate bending capacity (P_{nc}) is calculated as follows:

$$F_{s1} = F_{c1} \quad (8)$$

$$F_{s2} = F_{c2} \quad (9)$$

$$F_{s1} = F_{s21} = A_s f_y \quad (10)$$

$$F_{c1} = 0.85 f_c b x_1 \quad (11)$$

$$F_{c2} = 0.85 f_c b x_2 \quad (12)$$

where F_{s1} and F_{s2} are the tensile forces of the steel bars in the inner and outer concrete wythes, respectively, F_{c1} and F_{c2} are, respectively, the pressure on the concrete section of the inner and outer concrete wythes, A_s is the cross-sectional area of tensile reinforcement and x_1 and x_2 are, respectively, the compression height of inner and outer concrete wythes.

$$M_{nc} = F_{s1}\left(h_1 - \frac{x_1}{2}\right) + F_{s2}\left(h_2 - \frac{x_2}{2}\right) \quad (13)$$

$$P_{nc} = \frac{8M_{nc}}{l} \quad (14)$$

where M_{nc} is the ultimate bending moment of non-composite panels and h_1 and h_2 are, respectively, the distance from the stress reinforcement in the two concrete panels to the concrete's edge in the compression zone.

When the sandwich panel is a complete composite panel (Figure 14b), two concrete wythes bear the load together as an integral component, and the flexural bearing capacity (P_c) is calculated as follows:

$$F_s = F_c \quad (15)$$

$$M_c = F_s\left(h - \frac{x}{2}\right) \quad (16)$$

$$P_c = \frac{8M_c}{l} \quad (17)$$

where F_s is the tensile force of the tensile reinforcement, F_c is the pressure on the concrete section in the complete composite panel, M_c is the ultimate bending moment of the complete composite panel, h is the distance from the stressed reinforcement to the edge of the concrete and x is the compression height of the sandwich panel [27].

After the cracking of the specimen, the composite degree of the bearing capacity is used to represent it [38]:

$$k_2 = \frac{P_e - P_{nc}}{P_c - P_{nc}} \quad (18)$$

where P_e is the actual ultimate load of sandwich panel in the test.

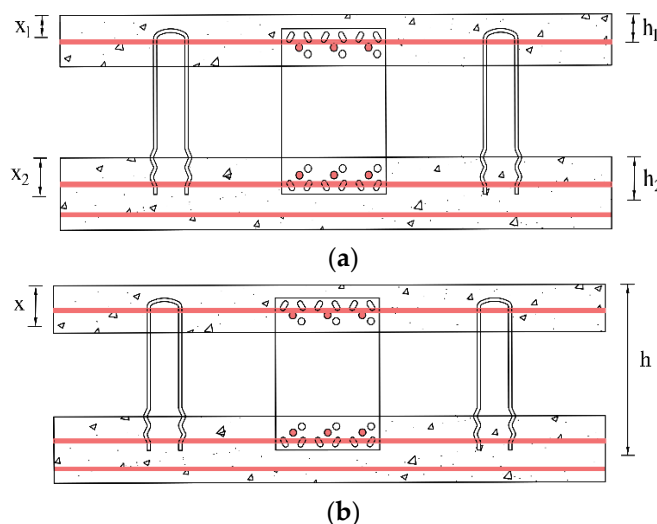


Figure 14. Theoretical calculation models: (a) non-composite panel; (b) complete composite panel.

According to the calculation results and the test data, the rigidity composite degree and bearing-capacity composite degree of each specimen can be obtained, as shown in Table 7.

Table 7. Calculation results of composite degrees of specimens.

Panels	$I_{nc}/10^7 \text{ mm}^4$	$I_c/10^8 \text{ mm}^4$	$I_{exp}/10^8 \text{ mm}^4$	$k_1/\%$	P_{nc}/kN	P_c/kN	P_e/kN	$k_2/\%$
SP-1	9.31	7.58	2.09	17.43	86.94	294.22	113.82	12.97
SP-2	7.09	5.38	1.78	22.94	65.03	263.46	103.11	18.70
SP-3	9.31	5.38	2.10	26.28	86.94	263.46	114.54	15.64
SP-4	9.31	7.58	2.13	17.96	86.94	294.22	115.67	13.86

According to Table 7, when the thickness of the inner concrete wythe is reduced by 20%, the composite degree of the rigidity and bearing capacity of the PCCISP can be increased by 5.51% and 5.73%, respectively. When the thickness of the insulation layer was reduced by 30%, its rigidity and bearing capacity composite degree increased by 8.85% and 2.67%, respectively. This was because a reduction in the thickness of the insulation layer can reduce the shear deformation between the two concrete wythes, and improve the load-transfer efficiency, so as to enhance the composite degree of the sandwich panel. When length of the plate-type shear connector was increased by 1.67 times, the rigidity and bearing capacity composite degree were increased by 0.53% and 0.89%, respectively.

6. Conclusions

Through the static testing and numerical simulation of bending for four precast ceramsite concrete sandwich panels, and the calculation and analysis of the composite degree of each specimen, the results are as follows:

- The failure modes of four precast ceramsite-concrete-insulated sandwich panels were all ductile failures of concrete flexural members, and all of them were partial composite panels.
- The load-deflection curve of PCCISP simulated by finite-element was in good agreement with the test curve, the simulated value of ultimate bearing capacity was close to the test value, and the finite-element model established was more accurate, which can be used as the basis for analyzing other working conditions of the same type of sandwich panel.
- With the decrease in the inner concrete wythe thickness, the overall rigidity and ductility of the PCCISP can decrease. When the thickness of the inner concrete wythe decreased by 20%, the cracking load decreased by 25.03% and the ultimate bearing capacity decreased by 9.41%. The ultimate bearing capacity was not significantly affected by reducing the thickness of the insulation layer. The ultimate bearing capacity can be slightly increased by increasing the length of the plate-type shear connector and the number of pin-type shear connectors.
- The composite degree of the rigidity and bearing capacity of PCCISP are increased when the thickness of the inner concrete wythe decreases. The thickness of the insulation layer was reduced, which can greatly improve the composite degree of rigidity, and the composite degree of the bearing capacity can be increased slightly. Increasing the length of the stainless steel plate-type shear connector had no obvious effect on the composite degree of rigidity and bearing capacity of PCCISP.

Author Contributions: Y.C. is responsible for project management and supervision. C.K. is responsible for writing and translation. Y.W. is responsible for making test plan and solving problems during the test. Z.Q. is responsible for the numerical simulation. All authors have read and agreed to the published version of the manuscript.

Funding: This work was funded by the National Natural Science Foundation of China (51668063).

Data Availability Statement: Not applicable.

Conflicts of Interest: The authors declare no conflict of interest.

References

1. Mobaraki, B.; Komarizadehasl, S.; Castilla Pascual, F.J.; Lozano-Galant, J.A.; Porras Soriano, R. A Novel Data Acquisition System for Obtaining Thermal Parameters of Building Envelopes. *Buildings* **2022**, *12*, 670. [\[CrossRef\]](#)
2. Konstantinou, T.; Knaack, U. Refurbishment of Residential Buildings: A Design Approach to Energy-Efficiency Upgrades. *Procedia Eng.* **2011**, *21*, 666–675. [\[CrossRef\]](#)
3. Ma, S.; Gu, Y.; Bao, P. Seismic performance of ceramsite concrete T-shaped composite wallboard joints under cyclic loading. *Structures* **2021**, *33*, 4433–4445. [\[CrossRef\]](#)
4. Qiu, J.; Xing, M.; Yang, Z.; Zhang, C.; Guan, X. Micro-pore structure characteristics and macro-mechanical properties of PP fibre reinforced coal gangue ceramsite concrete. *J. Build. Eng.* **2020**, *8*, 1192–1197. [\[CrossRef\]](#)
5. Bu, C.; Zhu, D.; Liu, L.; Lu, X.; Sun, Y.; Yan, Z.; Yu, L.; Wei, Q. A Study on the Mechanical Properties and Microcosmic Mechanism of Basalt Fiber Modified Rubber Ceramsite Concrete. *Buildings* **2022**, *12*, 103. [\[CrossRef\]](#)
6. Xie, J.; Zhao, J.; Wang, J.; Huang, P.; Liu, J. Investigation of the high-temperature resistance of sludge ceramsite concrete with recycled fine aggregates and GGBS and its application in hollow blocks. *J. Build. Eng.* **2020**, *34*, 101954. [\[CrossRef\]](#)
7. Li, X.; Yan, F.; Yue, X. Research progress of ceramsite concrete. *J. Bull. Chin. Ceram. Soc.* **2020**, *39*, 3407–3418, 3452.
8. Ma, S.C.; Li, L.H.; Bao, P. Seismic Performance Test of Double-Row Reinforced Ceramsite Concrete Composite Panels with Cores. *J. Appl. Sci.* **2021**, *11*, 2688. [\[CrossRef\]](#)
9. Aksakal, B.; Ulutaş, A.; Balo, F.; Karabasevic, D. A New Hybrid MCDM Model for Insulation Material Evaluation for Healthier Environment. *Buildings* **2022**, *12*, 655. [\[CrossRef\]](#)
10. Gama, N.V.; Ferreira, A.; Barros-Timmons, A. Polyurethane Foams: Past, Present, and Future. *Materials* **2018**, *11*, 1841. [\[CrossRef\]](#)
11. Yin, X.; Li, H.; Bo, H.; Ke, H. Weatherability studies on external insulation thermal system of expanded polystyrene board, polystyrene granule and polyurethane foam. *J. Wuhan Univ. Technol. Sci. Ed.* **2010**, *25*, 1027–1032. [\[CrossRef\]](#)
12. Kinnane, O.; West, R.; Hegarty, R.O. Structural shear performance of insulated precast concrete sandwich panels with steel plate connectors. *J. Eng. Struct.* **2020**, *215*, 110691. [\[CrossRef\]](#)
13. Einea, A.; Salmon, D.C.D.C.; Tadros, M.K.; Culp, T. A new structurally and thermally efficient precast sandwich panel system. *PCI J.* **1994**, *39*, 90–101. [\[CrossRef\]](#)

14. Portal, N.W.; Flansbjer, M.; Zandi, K.; Wlasak, L.; Malaga, K. Bending behaviour of novel Textile Reinforced Concrete-foamed concrete (TRC-FC) sandwich elements, *Compos. J. Struct.* **2017**, *177*, 104–118.
15. Huang, J.; Dai, J. Direct shear tests of glass fiber reinforced polymer connectors for use in precast concrete sandwich panels. *Compos. Struct.* **2019**, *207*, 136–147. [[CrossRef](#)]
16. Hassan, T.K.; Rizkalla, S.H. Analysis and design guidelines of precast, prestressed concrete, composite load-bearing sandwich panels reinforced with CFRP grid. *PCI J.* **2010**, *55*, 147–162. [[CrossRef](#)]
17. Kazem, H.; Bunn, W.G.; Seliem, H.M.; Rizkalla, S.H.; Gleich, H. Durability and long term behavior of FRP/foam shear transfer mechanism for concrete sandwich panels. *J. Constr. Build. Mater.* **2015**, *98*, 722–734. [[CrossRef](#)]
18. Carbonari, G.; Cavalaro, S.H.P.; Cansario, M.M. Flexural behavior of light-weight sandwich panels composed by concrete and EPS. *J. Constr. Build. Mater.* **2012**, *35*, 792–799. [[CrossRef](#)]
19. Zhang, J.; Qin, Q.; Ai, W.; Li, H.; Wang, T.J. The failure behavior of geometrically asymmetric metal foam core sandwich beams under three-point bending. *J. Appl. Mech.* **2014**, *81*, 071008. [[CrossRef](#)]
20. Zhang, J.; Qin, Q.; Han, X.; Ai, W. The initial plastic failure of fully clamped geometrical asymmetric metal foam core sandwich beams. *Compos. Part B Eng.* **2016**, *87*, 233–244. [[CrossRef](#)]
21. Zhang, J.; Ye, Y.; Qin, Q. Large deflections of multilayer sandwich beams with metal foam cores under transverse loading. *Acta Mech.* **2018**, *229*, 3585–3599. [[CrossRef](#)]
22. Zhang, J.; Sun, H.; Du, J. Large deflection of multilayer sandwich beams with foam-filled trapezoidal corrugated and foam cores. *Thin Walled Struct.* **2022**, *179*, 109755. [[CrossRef](#)]
23. Bush, T.; Stine, G. Flexural behavior of composite precast concrete sandwich panels with continuous truss connectors. *PCI J.* **1994**, *3*, 112–121. [[CrossRef](#)]
24. Huang, J.; Jiang, Q.; Chong, X. Experimental study on precast concrete sandwich panel with cross-shaped GFRP connectors. *Adv. Struct. Eng.* **2020**, *72*, 149–162. [[CrossRef](#)]
25. Zhi, Q.; Guo, Z. Experimental evaluation of precast concrete sandwich panels with steel–glass fiber–reinforced polymer shear connectors. *Adv. Struct. Eng.* **2017**, *20*, 1476–1492. [[CrossRef](#)]
26. O’Hegarty, R.; West, R.; Reilly, A.; Kinnane, O. Composite behaviour of fibre-reinforced concrete sandwich panels with FRP shear connectors. *J. Eng. Struct.* **2019**, *198*, 109475. [[CrossRef](#)]
27. Choi, I.; Kim, J.; Kim, H.-R. Composite behavior of insulated concrete sandwich panels subjected to wind pressure and suction. *Materials* **2015**, *8*, 1264–1282. [[CrossRef](#)]
28. Frankl, B. Behavior of insulated precast prestressed concrete sandwich panels reinforced with CFRP grid—Masters Thesis. Ph.D. Thesis, North Carolina State University, Raleigh, NC, USA, 2008.
29. Pessiki, S.; Mlynarczyk, A. Experimental evaluation of the composite behavior of precast concrete sandwich panels. *PCI J.* **2003**, *48*, 54–71. [[CrossRef](#)]
30. Wang, Y.; Yu, T.; Zhang, L.; Yin, L.; Wu, Y.; Chen, B. Fatigue Performance of Rib Beam Bridge Slabs Reinforced with Polyurethane Concrete Based on the Damage Theory. *Buildings* **2022**, *12*, 704. [[CrossRef](#)]
31. Wang, W.; Zhang, X.; Ren, Y.; Bai, F.; Li, C.; Li, Z. Finite Element Modelling of Bolt Shear Connections in Precast Steel Lightweight Aggregate–Concrete Composite Beams. *Buildings* **2022**, *12*, 758. [[CrossRef](#)]
32. Gombeda, M.; Trasborg, P.; Naito, C.J. Simplified model for partially-composite precast concrete insulated panels subjected to lateral loading. *J. Eng. Struct.* **2017**, *138*, 367–380. [[CrossRef](#)]
33. Hodicky, K.; Sopal, G.; Rizkalla, S.; Hulin, T.; Stang, H. Experimental and numerical investigation of the FRP shear mechanism for concrete sandwich panels. *Compos. Constr.* **2015**, *19*, 04014083. [[CrossRef](#)]
34. Tomlinson, D.; Fam, A. Analytical approach to flexural response of partially composite insulated concrete sandwich walls used for cladding. *J. Eng. Struct.* **2016**, *122*, 251–266. [[CrossRef](#)]
35. Chen, A.; Yossef, M.; Hopkins, P. A comparative study of different methods to calculate degrees of composite action for insulated concrete sandwich panels. *J. Eng. Struct.* **2020**, *212*, 110423. [[CrossRef](#)]
36. Insub, C.; Jun-Hee, K.; Young-Chan, Y. Effect of cyclic loading on composite behavior of insulated concrete sandwich panels with GFRP shear connectors. *Compos. Part B Eng.* **2016**, *96*, 7–19.
37. Benayoune, A.; Samad, A.A.; Trikha, D.; Ali, A.A.; Ellinna, S. Flexural behaviour of pre-cast concrete sandwich composite panel—experimental and theoretical investigations. *Constr. Build. Mater.* **2008**, *22*, 580–592. [[CrossRef](#)]
38. Huang, J.; Dai, J. Flexural performance of precast geopolymer concrete sandwich panel enabled by FRP connector. *Compos. Struct.* **2020**, *248*, 112563. [[CrossRef](#)]